Journal of Medicinal and Nanomaterials Chemistry 6 (2024) 1-11

Journal of Medicinal and Nanomaterials Chemistry

Journal homepage: https://jmnc.samipubco.com/

Original Research Article

Fabrication of various morphologies of MnO_2 nanostructures on biochar support for dye removal application

Maryam Fayazi *

Department of Environment, Institute of Science and High Technology and Environmental Sciences, Graduate University of Advanced Technology, Kerman, Iran

ARTICLE INFORMATION

Received: 19 November 2023
Received in revised: 29 December 2023
Accepted: 08 January 2024
Available online: 10 January 2024

DOI: 10.4839/JMNC.2024.1.1

KEYWORDS

Removal
Biochar
Methylene blue
Manganese dioxide
Morphology

ABSTRACT

Biochar is a cost-effective and porous material with high carbon content. It is considered as an effective supporting matrix owing to its high specific surface area and notable ion exchange ability. In this work, a porous biochar support was fabricated from pistachio residues using pyrolysis procedure. Subsequently, various crystalline phases and morphologies of MnO_2 were deposited onto the biochar support through chemical protocols with $Mn(Ac)_2$, $KMnO_4$, and $MnSO_4$ as Mn source. The N_2 adsorption-desorption experiments were employed to characterize the porosities and specific surface areas of the synthesized nanocomposites. It is found that the γ-MnO_2/biochar composite possessed the higher surface area than the δ-MnO_2 and α-MnO_2 samples. The adsorption features of the composite materials in the removement of target dye from aqueous solution were also examined. Based on the experimental results, the γ-MnO_2/biochar sample showed the highest efficiency for removal of target dye. In addition, the experimental data exhibited a good correlation (R^2 greater than 0.99) with the pseudo-second-order kinetic model, indicating a chemical adsorption approach for dye adsorption.

Corresponding author, email: maryam.fayazi@yahoo.com, m.fayazi@kgut.ac.ir (M. Fayazi).

Graphical Abstract

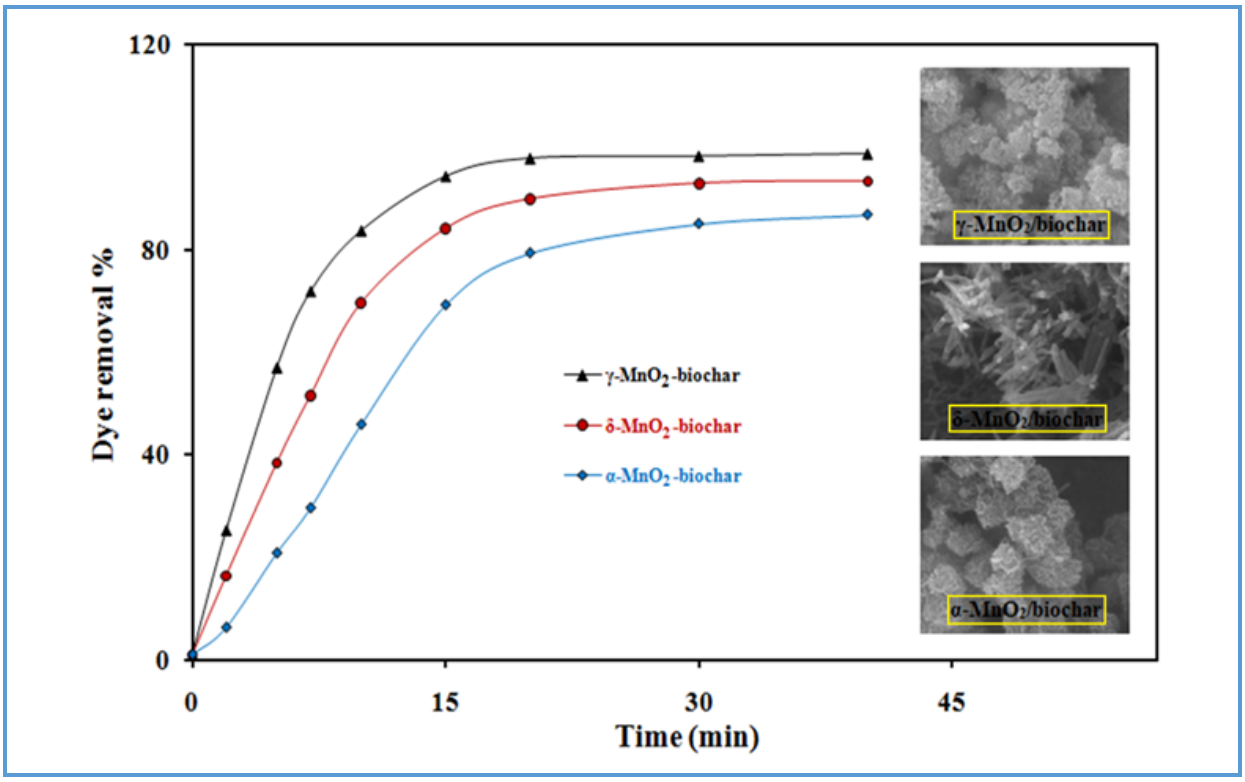

Introduction

Over the past few years, nano-sized metal oxides have become a subject of great interest because of their considerable features that distinguish them from micro-sized materials [1-3]. Manganese oxide (MnO_2) is a fascinating metal oxide material that exhibits a multitude of structures and possesses a range of chemical characters [4,5]. Concrning its low cost and environmental friendliness, MnO_2 has been employed in the wide range of applications including catalysis, sensor and energy storage [6-8]. Generally, the performance of MnO_2 compounds is highly influenced by their morphologies and crystallographic structures. In this context, several synthetic procedures (viz., chemical, photo-chemical, green, and electrochemical) have been successfully researched for the synthesis of MnO_2 products [9-12]. Discharge of dye-containing wastewaters is causing significant issues for both human health and the environment nowadays [13-16]. Facing this environmental issue, the adsorption strategy has been used as a promising treatment method due its remarkable advantages such as cost-effectiveness, simplicity in operation, sludge-free operation, and sorbent reusability [17,18]. Recently, MnO_2 nanostructures have been employed as the efficient adsorbents in water treatment applications due to their unique physical and chemical properties [19,20]. However, the utilization of pure nano-sized MnO_2 as an adsorbent is not economically viable and possesses unfavorable physiochemical properties [21]. To solve the aforesaid challenges, MnO_2 can be deposit on the various support substrates, which significantly influences the sorption

performance of the composite adsorbents [22,23]. Recently, some researchers used the hybrid sorbents based on deposition of MnO_2 on carbon supports such as carbon nanotube (CNT) and graphene oxide (GO), which illustrate significant improvements in removal efficiency [24,25]. However, the employment of CNT and GO as adsorbent supports is not economically beneficial.

Nowadays, biochar has emerged as one of the most widely used supports for metal/metal oxide particles, owing to its higher surface area and ion-exchange capacity among various available supports [26-28]. Biochar is a porous and stable solid material high carbon content. Usually, biochar materials are produced by converting carbonaceous biomass through thermochemical methods such as pyrolysis and hydrothermal carbonization in an oxygen-limited or oxygen free atmosphere [29]. Biochar can be prepared using various organic wastes like agricultural wastes, garden residues, municipal wastes, and algae [30,31]. Biochar is characterized by its high carbon content, diverse functional groups, superior surface-area-to-volume ratio, chemical and mechanical constancy, and impressive adsorption ability [32]. In addition, biochar was found to be more economical than some of the other carbon substances like GO and CNT. Accordingly, these points, biochar can be employed as a promising adsorbent to remove organic contaminant and heavy metals from polluted water resources [33,34].

In this work, to combine the advantages of biochar and metal oxide particles, we fabricated various MnO_2/biochar nanocomposites and applied them as adsorbents for dye removal. To reach this goal, the pistachio residues were initially used as raw material to fabricate the porous biochar support.

Then, MnO_2 with different morphologies (wire, spherical, and flower-like) and crystalline forms (δ, α, and γ), was deposited on the surface of biochar throughout the hydrothermal and precipitation procedures. The prepared MnO_2-biochar was characterized using scanning electron microscope (SEM), X-ray diffraction (XRD), and Brunauer-Emmett-Teller (BET) methods. The performance of the prepared composite adsorbent for removal of methylene blue (MB) was studied and discussed.

Experimental

Materials and instruments

Chemicals (analytical grade) including manganese (II) sulfate monohydrate ($MnSO_4.H_2O$), potassium permanganate ($KMnO_4$), MB, ammonium persulfate ($(NH_4)_2S_2O_8$), manganese (II) acetate tetrahydrate ($Mn(CH_3CO_2)_2.\ 4H_2O$) were obtained from Merck (Darmstadt, Germany), and used without any purification. In all synthesis procedures and catalytic tests, distilled water was utilized. Pistachio samples were harvested from pistachio trees in Sirjan City (Kerman Province, Iran).

The concentrations of target dye were determined by using UV-Vis spectrophotometer (Cary 50, Varian, Australia). XRD patterns were recorded on a PANalytical Empyrean X-ray diffractometer (Almelo, Netherlands) with a Cu-Ka radiation (λ=0.15418 nm). The morphologies of the prepared MnO_2/biochar nanocomposites were evaluated using SEM analysis on a MIRA3 LM TESCAN microscope (Brno, Czech Republic). The specific surface areas of the sorbents were studied using the BET measurements on a using a Belsorp-mini II (BEL Japan, Inc.) instrument at 77 K. All samples were initially

heat treated under vacuum at 473 K for 6 h before the adsorption measurement.

Preparation of biochar

Biochar support was fabricated according to a previously reported method [35]. Firstly, the moisture content of clean pistachio shells was removed heat treatment at 110 °C for 12 h. The obtained shells were crushed with a coffee grinder, and then pyrolyzed at 750 °C under N_2-purged condition in a muffle furnace for 1 h.

Preparation of MnO_2-biochar nanostructures

The MnO_2-biochar nanocomposites with various crystalline phases and morphologies were formed with the hydrothermal and precipitation strategies according to following procedures.

To prepare the flower-like α-MnO_2-biochar nanocomposite, 2.0 g of biochar sample was dispersed in 30 mL of distilled water under ultra-sonication for 15 min. Subsequently, 20 mL of Mn(II) solution containing 2.79 g $Mn(CH_3CO_2)_2$ was dropwisely added to above mixture. After magnetic stirring for 30 min, 1.2 g of $KMnO_4$ was dissolved in 20 mL pure water and this solution was added to the biochar suspension and the mixture was again stirred for 10 min, followed with the hydrothermal treatment at 80°C for 4 h in a a Teflon-lined stainless-steel autoclave (100 mL). After cooling, the product was filtered, thoroughly rinsed with distilled water and then dried at 60 °C for 10 h.

To prepare the wire-like δ-MnO_2-biochar nanocomposite, 2.0 g of biochar sample was initially sonicated in 30 mL of distilled water. Separately, 2.21 g of $KMnO_4$ and 3.19 g of $(NH_4)_2S_2O_8$ were dissolved into 20 mL of distilled water, and then the $KMnO_4$ solution was added to the biochar suspension drop by drop under stirring. After that, the $(NH_4)_2S_2O_8$ solution was added to the above mixture and the mixture was stirred continuously for 30 min. The achieved mixture was subjected to a 100 mL autoclave and then maintained in an oven at 90 °C for 12 h. The precipitate was filtered, washed with distilled water 3 times, and then dried at 60 °C for 10 h.

To prepare the spherical-like γ-MnO_2-biochar nanocomposite, 2.0 g of biochar sample was well dispersed in 70 mL of distilled water. Afterwards, 0.32 g of $KMnO_4$ and 0.50 g of $MnSO_4.H_2O$ was put into the prepared biochar suspension and magnetic stirred for 6 h under ambient condition. The obtained product was filtered, thoroughly rinsed with pure water, and then dried in an oven at 60 °C for 10 h.

Results and Discussion

Characterization

Figure 1 displays the XRD patterns of the different MnO_2-biochar nanocomposites. The XRD pattern of biochar sample illustrates no clear reflections of the crystalline phases and two broad peaks at 24.1° and 43.2° are attributed to graphitic carbon structures [36]. In wire-like MnO_2-biochar nanocomposite, the diffraction peaks at 2θ values of 12.3°, 26.5°, 37.8°, 41.2°, 54.9°, 59.5°, and 65.2° can be well indexed to δ-MnO_2 (JCPDS no. 80-1098) [37]. The flower-like MnO_2-biochar sample depicts some diffraction peaks at 2θ= 12.6°, 28.3°, 38.2°, 41.2°, 50.0°, 60.0°, and 65.9°, which can be indexed to α-MnO_2 phase (JCPDS no. 44-0141) [38]. The spherical-like MnO_2-biochar nanocomposite displayed the distinct diffraction peaks at 2θ= 22.9°, 37.5°, 42.9°, and 66.8°, mainly attributable to γ-MnO_2 crystalline phase (JCPDS no. 14-0644) [39]. Based on the Scherrer formula: $D= 0.89\lambda/\beta\cos\theta$ [40,41], where D is the average crystal size, λ is the Cu-Kα wavelength (0.15406 nm), β is the half-

width of the peak in radians, and θ is the corresponding diffraction angle, the average crystallite sizes of the δ-MnO_2, α-MnO_2, and γ-MnO_2 particles calculated from the XRD patterns are about 44.6 nm, 27.5 nm, and 38.2 nm, respectively. The SEM analysis of biochar and MnO_2-biochar nanostructures are illustrated in Figure 2. As depicted in Figure 2A, the biochar sample has fairly smooth surface.

The MnO_2-biochar nanostructures have a rougher surface compared to biochar, indicating the MnO_2 particles has been randomly deposited on the carbon support. Also, the different shapes of MnO_2 consisting of wire- (Fig. 2B), flower- (Fig. 2C), and spherical-like (Fig. 2D) successfully deposited on the surface of biochar, which are correspond to the δ-, α- and γ-MnO_2 phases, respectively. The N_2 adsorption/desorption isotherms of the biochar and MnO_2-biochar nanostructures at 77 K are displayed in Figure 3. The type-I behavior of the isotherm indicates that the biochar is a microporous support material. The isotherms of MnO_2-biochar nanocomposites present a steep increase in N_2 uptake in the initial part, revealing the presence of micropores.

In addition, both micropores and mesopores are observed by the isotherms at high relative pressure. From this perspective, the fabricated nanocompositte possess both micro- and meso- porosity. Besides, the specific surface area of γ-MnO_2-biochar (456 m^2 g^{-1}) is greater than the specific surface areas of δ-MnO_2-biochar (385 m^2 g^{-1}) and α-MnO_2-biochar (351 m^2 g^{-1}) samples. The obtained outcomes demonstrated that the γ-MnO_2-biochar is more porous than other prepared nanocomposites.

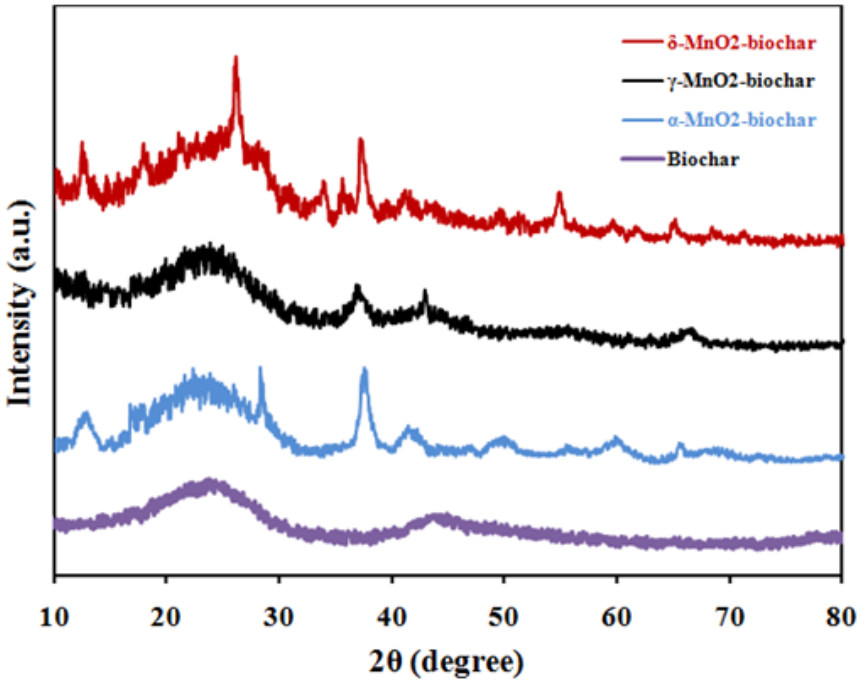

Figure 1. XRD patterns of biochar and MnO_2-biochar nanocomposites.

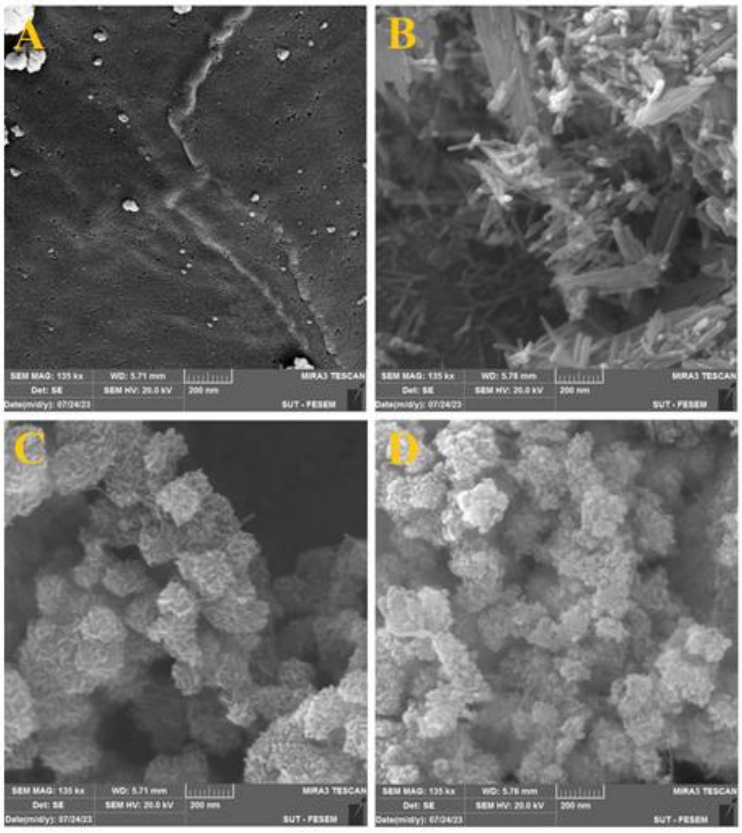

Figure 2. SEM images of (A) biochar, (B) δ-MnO_2-biochar, (C) α-MnO_2-biochar, and (D) γ-MnO_2-biochar samples.

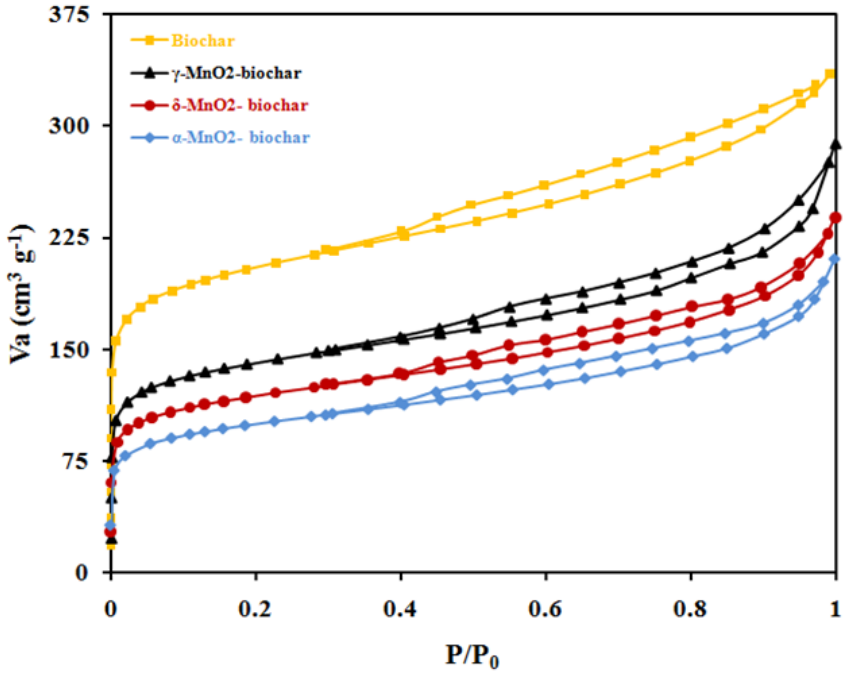

Figure 3. N_2 adsorption/desorption isotherms of biochar and various MnO_2-biochar nanocomposites at 77 K.

Adsorption studies

Dye adsorption tests were performed in 50 mL Erlenmeyer flasks containing 20 mL dye solution. This mixture was agitated for 20 min using a shaker at 350 rpm. After the assumed adsorption time, the MnO_2-biochar sorbents were collected and the absorbance was measured.

The residual concentration of the dye in the residual MB concentration was then measured using the UV-Vis spectrophotometer at 655 nm. The percentage removal of MB was calculated using Equation (1) [42]:

$$\text{Removal efficiency} = \frac{C_0 - C_t}{C_0} \times 100 \qquad (1)$$

Where, C_0 and C_t are the initial and final concentrations of MB (mg L^{-1}), respectively.

The performances of various MnO_2/biochar nanostructures towards MB removal were explored and the results are depicted in Figure 4A. Within 20 min reaction time, the removal efficiencies of the adsorbent materials were 97.8%, 89.8%, and 79.3% over γ-, δ- and α-MnO_2, respectively. The fast MB removal by γ-MnO_2-biochar can be explained by its higher specific surface area that provides more adsorption centers at the initial stages. In addition, the MB uptake was quick in the first 20 min, and then occurred in the slow manner until the absorption equilibrium. The initial fast adsorption can be explained by the abundance of adsorption sites in the nanocomposite sorbents. However, as more sites get occupied, repulsion interactions occur between the surface MB molecules and the bulk solution [43,44]. UV-Vis spectral changes of the MB removal process by γ-MnO_2-biochar are depicted in Figure 4B. Obviously, a rapid decrease in the absorption band of MB at 665 nm was observed over time. The absence of any changes in peak position or the appearance of new absorption bands suggests that no intermediates were present in the course of MB removal. As you can seen in inset of Figure 4B, the color of MB solution is change from deep blue to pale blue within 20 min when exposes by γ-MnO_2-biochar sorbent.

Adsorption kinetics

The adsorption kinetics was explored using two common models, the pseudo-first-order (PFO) and pseudo-second-order (PSO) kinetic models (Equations (2) and (3)). PFO kinetic model can be expressed as follow [45]:

$$\ln(q_e - q_t) = \ln q_e - k_1 t \qquad (2)$$

PSO kinetic model can be described as follow [46]:

$$\frac{t}{q_t} = \frac{1}{k_2 q_e^2} + \frac{1}{q_e} t \qquad (3)$$

Where, q_e (mg g^{-1})=equilibrium amount of adsorbed MB, q_t (mg g^{-1})=amount of adsorbed MB at time, k_1 (min^{-1})=PFO rate constant, and k_2 (g $mg^{-1}min^{-1}$)=PSO rate constant. Table 1 presents the kinetic constants achieved by both kinetic models. The correlations of the kinetic data derived by PFO and PSO models are demonstrated in Figure 5 A and B. Obviously, the PSO kinetic model could provide a better description for MB uptake using γ-, δ-, and α-MnO_2-biochar materials with R^2 values >0.999, which suggest the removal process occurs through chemical adsorption.

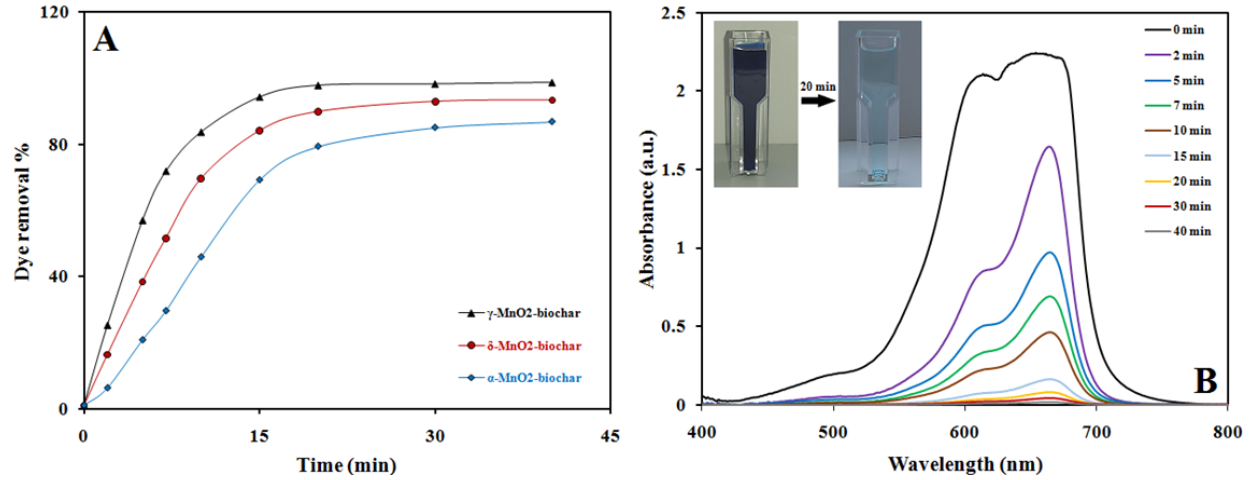

Figure 4. (A) Removal of MB by various nanostructures as a function of contact time (Initial dye concentration: 50 mg L^{-1}, T=298 K, sorbent dose = 0.01 g) (the right side) and (B) UV-Vis spectra of MB dye solution at various intervals treated by γ-MnO_2-biochar. Inset in Figure 4B shows digital pictures of the MB dye before and after treatment with the γ-MnO_2-biochar within 20 min.

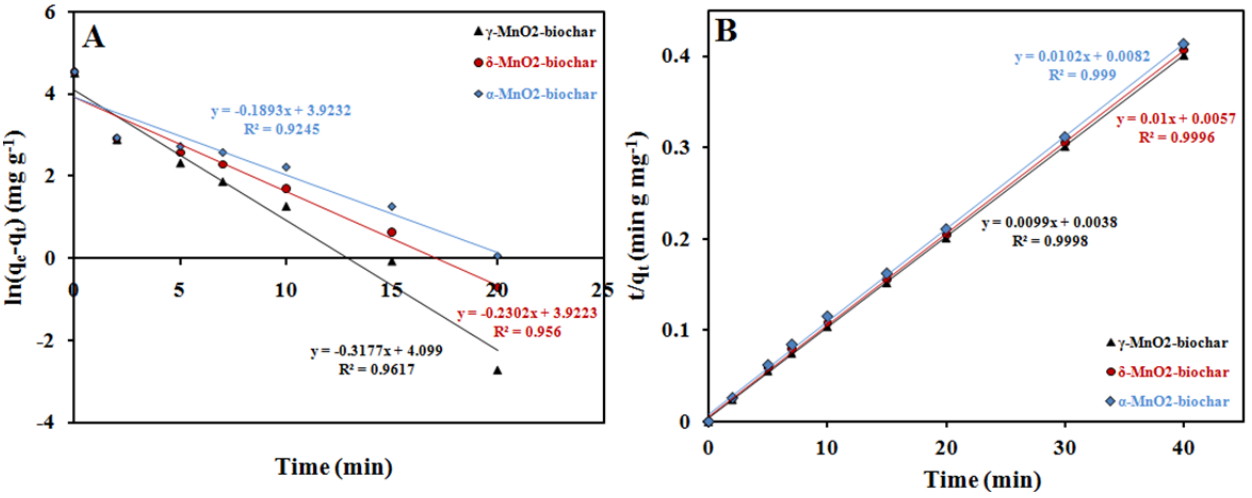

Figure 5. (A) PFO and (B) PSO kinetic models for MB adsorption using different MnO_2-biochar adsorbents.

Table 1. Kinetic parameters of PFO and PSO models for MB uptake by MnO_2-biochar nanocomposites

	Pseudo-first-order				Pseudo-second-order		
Sorbent	$q_{e,exp}$ (mg g^{-1})	$q_{e,cal}$ (mg g^{-1})	k_1 (min^{-1})	R^2	$q_{e,cal}$ (mg g^{-1})	k_2 (g mg^{-1} min^{-1})	R^2
α-MnO_2-biochar	96.0	50.6	0.1893	0.9245	98.0	0.013	0.9990
δ- MnO_2-biochar	98.1	50.5	0.2302	0.9560	100.0	0.017	0.9996
γ-MnO_2-biochar	99.5	60.3	0.3177	0.9617	101.0	0.026	0.9998

Conclusion

To sum up, MnO_2 nanostructures with different phase and morphologies were successfully prepared on the surface of pistachio residues biochar. The physicochemical properties of the MnO_2-biochar nanocomposites were characterized using XRD, SEM, and BET analyses. The SEM and XRD data indicated that the prepared MnO_2 with hydrothermal and precipitation methods have different shapes (wire-, flower-, and spherical-like) and crystalline structures (δ-, γ-, and α-MnO_2). The BET studies show that the γ-MnO_2-biochar higher specific surface compared to δ- and α-MnO_2-biochar sorbents. This finding can justify the better adsorption performance of the spherical-like γ-MnO_2-biochar for MB elimination. The γ-MnO_2-biochar illustrated the remarkable removal efficiency more than 97 % after 20 min for target dye.

The advantages of the MnO_2-biochar adsorbents include simple preparation, relatively low cost, and high adsorption efficiency. To the best of our knowledge, there is no report on pistachio based biochar loaded with different shapes of MnO_2 toward dye pollutant removal.

Orcid

Maryam Fayazi : 0000-0002-9385-136X

References

[1]. Zhang F., Zhou Y.k., Li H. *Mater. Chem. Phys.*, 2004, **83**:260 [Crossref], [Google Scholar], [Publisher]

[2]. Saadh M.J., Roy H., Ademi E. *J. Med. Pharm. Chem. Res,.* 2022, **4**:1033 [Crossref], [Google Scholar]

[3]. Ikhioya I.L., Rufus I., Ifeyinwa Akpu N., *J. Med. Nanomater. Chem*., 2022, **4**:88 [Crossref], [Publisher]

[4]. Fathy N.A., El-Shafey S.E., El-Shafey O.I., Mohamed W.S. *J. Environ. Chem. Eng.*, 2013, **1**:858 [Crossref], [Google Scholar], [Publisher]

[5]. Abegunde S.M., Idowu K.S. *Eurasian J. Sci. Technol.*, 2023, **3**:109 [Crossref], [Publisher]

[6]. Xu J.J., Zhao W., Luo X.L., Chen H.Y. *Chem. Comm*., 2005, 792 [Crossref], [Google Scholar], [Publisher]

[7]. Lume-Pereira C., Baral S., Henglein A., Janata E. *J. Phys. Chem.*, 1985, **89**:5772 [Crossref], [Google Scholar], [Publisher]

[8]. Horváth O., Strohmayer K. *J. Photochem. Photobiol., A*, 1998, **116**:69 [Crossref], [Google Scholar], [Publisher]

[9]. Wang X., Li Y. *J. Am. Chem. Soc.*, 2002, **124**:2880 [Crossref], [Google Scholar], [Publisher]

[10]. Wu M.S., Lee J.T., Wang Y.Y., Wan C.C. *J. Phys. Chem. B*., 2004, **108**:16331 [Crossref], [Google Scholar], [Publisher]

[11]. Wang L., Ebina Y., Takada K., Sasaki T. *Chem. Comm.*, 2004, 1074 [Crossref], [Google Scholar], [Publisher]

[12]. Lu H., Zhang X., Khan S.A., Li W., Wan L. *Front. Microbiol.*, 2021, **12**:761084 [Crossref], [Google Scholar], [Publisher]

[13]. Pandey A., Singh P., Iyengar L. *Int. Biodeter. Biodegr*., 2007, **59**:73 [Crossref], [Google Scholar], [Publisher]

[14]. Bagheri Sadr M., Samimi A., *Adv. J. Chem., Sect. B,* 2022, **4**:174 [Crossref], [Publisher]

[15]. Aboshaloa E., Asweisi A., Almusrati A., Almusrati M., Aljhane H. *J. Med. Nanomater. Chem*., 2022, **5**:234 [Crossref], [Publisher]

[16]. Mohammed Alkherraz A., Elsherif K.M., El-Dali A., Blayblo N.A., Sasi M. *J. Med. Nanomater. Chem.,*. 2022, **4**:118 [Crossref], [Publisher]

[17]. Fayazi M., Ghanei-Motlagh M., Taher M.A. *Mater. Sci. Semicond. Process.*, 2015, **40**:35 [Crossref], [Google Scholar], [Publisher]

[18]. Fayazi M. *Environ. Sci. Pollut. Res.*, 2020, **27**:12270 [Crossref], [Google Scholar], [Publisher]
[19]. Yang R., Fan Y., Ye R., Tang Y., Cao X., Yin Z., Zeng Z. *Adv. Mater.*, 2021, **33**:2004862 [Crossref], [Google Scholar], [Publisher]
[20]. Zhai R., Wan Y., Liu L., Zhang X., Wang W., Liu J., Zhang B. *Water Sci. Technol.*, 2012, **65**:1054 [Crossref], [Google Scholar], [Publisher]
[21]. Rodriguez-Narvaez O.M., Peralta-Hernandez J.M., Goonetilleke A., Bandala E.R. *J. Ind. Eng. Chem*., 2019, **78**:21 [Crossref], [Google Scholar], [Publisher]
[22]. Afzali D., Fayazi M. *J. Taiwan Inst. Chem. Eng*., 2016, **63**:421 [Crossref], [Google Scholar], [Publisher]
[23]. Li J., Cai X., Liu Y., Gu Y., Wang H., Liu S., Liu S., Yin Y., Liu S. *Front. Environ. Sci.*, 2020, **8**:62 [Crossref], [Google Scholar], [Publisher]
[24]. Moghaddam H.K., Pakizeh M. *J. Ind. Eng. Chem.*, 2015, **21**:221 [Crossref], [Google Scholar], [Publisher]
[25]. Liu Y., Luo C., Cui G., Yan S. *RSC adv.*, 2015, **5**:54156 [Crossref], [Google Scholar], [Publisher]
[26]. Premarathna K., Rajapaksha A.U., Sarkar B., Kwon E.E., Bhatnagar A., Ok Y.S., Vithanage M. *Chem. Eng. J.*, 2019, **372**:536 [Crossref], [Google Scholar], [Publisher]
[27]. Wang S., Zhao M., Zhou M., Li Y.C., Wang J., Gao B., Sato S., Feng K., Yin W., Igalavithana A.D. *J. Hazard. Mater.*, 2019, **373**:820 [Crossref], [Google Scholar], [Publisher]
[28]. Thines K., Abdullah E., Mubarak N., Ruthiraan M. *Renew. Sust. Energ. Rev.*, 2017, **67**:257 [Crossref], [Google Scholar], [Publisher]
[29]. Wang J., Wang S. *J. Clean. Prod.*, 2019, **227**:1002 [Crossref], [Google Scholar], [Publisher]
[30]. Li L., Zou D., Xiao Z., Zeng X., Zhang L., Jiang L., Wang A., Ge D., Zhang G., Liu F. *J. Clean. Prod.*, 2019, **210**:1324 [Crossref], [Google Scholar], [Publisher]
[31]. Al-Layla A.M., Fadhil A.B. *Chem. Methodol.,* 2022, **6**:10 [Crossref], [Publisher]
[32]. Dai Y., Zhang N., Xing C., Cui Q., Sun Q. *Chemosphere*, 2019, **223**:12 [Crossref], [Google Scholar], [Publisher]
[33]. Ahmad M., Rajapaksha A.U., Lim J.E., Zhang M., Bolan N., Mohan D., Vithanage M., Lee S.S., Ok Y.S. *Chemosphere*, 2014, **99**:19 [Crossref], [Google Scholar], [Publisher]
[34]. Tan X., Liu Y., Zeng G., Wang X., Hu X., Gu Y., Yang Z. *Chemosphere*, 2015, **125**:70 [Crossref], [Google Scholar], [Publisher]
[35]. Nejadshafiee V., Islami M.R. *Environ. Sci. Pollut. Res.*, 2020, **27**:1625 [Crossref], [Google Scholar], [Publisher]
[36]. Fayazi M., Ghanei-Motlagh M. *J. Colloid Interface Sci.*, 2021, **604**:517 [Crossref], [Google Scholar], [Publisher]
[37]. Nawaz F., Cao H., Xie Y., Xiao J., Chen Y., Ghazi Z.A. *Chemosphere*, 2017, **168**:1457 [Crossref], [Google Scholar], [Publisher]
[38]. Devaraj S., Munichandraiah N. *J. Phys. Chem. C*, 2008, **112**:4406 [Crossref], [Google Scholar], [Publisher]
[39]. Revathi C., Kumar R.R. *Electroanalysis*, 2017, **29**:1481 [Crossref], [Google Scholar], [Publisher]
[40]. Mendoza R., Rodriguez-Gonzalez V., Zhakidov A., Cherepanov S., Mtz-Enriquez A., Oliva J. *J. Phys. D: Appl. Phys.*, 2021, **54**:315502 [Crossref], [Google Scholar], [Publisher]
[41]. Taeh A.S., Abdul-Hamead A.A., Othman F.M. *Chem. Methodol.,* 2022, **6**:428 [Crossref], [Publisher]
[42]. Fayazi M., Afzali D., Taher M., Mostafavi A., Gupta V. *J. Mol. Liq.*, 2015, **212**:675 [Crossref], [Google Scholar], [Publisher]
[43]. Diao H., Zhang Z., Liu Y., Song Z., Zhou L., Duan Y., Zhang J. *Cellulose*, 2020, **27**:7053 [Crossref], [Google Scholar], [Publisher]

[44]. Parekh P., Parmar A., Chavda S., Bahadur P. *J. Dispers. Sci. Technol*., 2011, **32**:1377 [Crossref], [Google Scholar], [Publisher]
[45]. Fayazi M., Ghanbarian M. *Silicon*, 2020, **12**:125 [Crossref], [Google Scholar], [Publisher]
[46]. Fayazi M. *Anal. Bioanal. Chem. Res.*, 2019, **6**:125 [Crossref], [Google Scholar], [Publisher]

How to cite this manuscript: Maryam Fayazi*. Fabrication of various morphologies of MnO_2 nanostructures on biochar support for dye removal application. *Journal of Medicinal and Nanomaterials Chemistry* , 2024, 6(1), 1-11. DOI: 10.4839/JMNC.2024.1.1